ECOLE POLYTECHNIQUE FEDERALE DE LAUSANNE
FACULTE DES SCIENCES DE LA VIE

Projet de master en Bioingénierie et Biotechnologie

3D multi-chamber fluidic systems for analysis of angiogenesis in biomaterials: Development, characterization and applications

Réalisé par

Carmen Bonvin

sous la direction du

Prof. Melody Swartz

et la supervision du

Dr. Adrian Shieh

au Laboratory of Lymphatic and Cancer Bioengineering (LLCB)
de l'EPFL

Expert externe
Dr. Algirdas Ziogas

LAUSANNE, EPFL 2009

3D multi-chamber fluidic systems for analysis of angiogenesis in biomaterials: Development, characterization and applications

Carmen Bonvin

Sentier de Renges 4bis, 1026 Denges

Contents

1 Summary

The cellular processes leading to capillary morphogenesis depend on external stimuli, in particular flow and morphogen gradients. Several devices have been designed to study these interactions *in vitro*. However, most of these devices allow a single experiment at a time, making it difficult to compare multiple conditions, which is needed for most biology experiments. Furthermore, it can be of great interest to use the same set of cells. Here we present two multi-chamber interstitial flow systems for side-by-side culture with the capability to follow the dynamics of individual cells. While a 9-chamber system was designed for cell culture or co-culture under radial flow, a multi-chamber migration assay allows studying cell migration into biomaterials under a constant flow profile. The effects of flow on lymphatic and blood endothelial cell morphology, as well as the extent of organization induced by VEGF, were observed. In addition, we demonstrated the feasibility of studying cell-cell interactions as well as cell-matrix interactions in a fibroblast and tumor cell co-culture. The two systems presented will allow for the study of interstitial flow and its effects.

2 Introduction

In vivo, cells reside in a complex microenvironment, made up of many cell types, an extracellular matrix (ECM), and signaling molecules such as growth factors and chemokines. Although two-dimensional (2D) cell cultures have proven their usefulness in biology, the multitudinous interactions involved in the microenvironment, including cell-cell and cell-matrix interactions as well as morphogen gradients, are better mimicked in three-dimensional (3D) cultures, making them more accurate for cell organization studies [27] [11] [43]. Cells in a 3D environment have an additional dimension to sense chemical or mechanical signals, which allows for polarization of cells, a process often needed for organization [12] [30]. Also, it allows gradient formation, and having an ECM matrix permits use of matrix-binding growth factors.

One of the key aspects of the cellular microenvironment is interstitial flow (IF). IF is caused by fluid leaking out of blood vessels. This fluid flow transports proteins and large molecules to interstitial cells and eventually lymphatic vessels that act as drains and bring this fluid back to the blood circulation. It is driven by the pressure difference between the blood circulation, the interstitum and the lymphatic vessels (Fig. 1) [26]. If nutrients do not leak out of the blood vessels, the tissue becomes necrotic and if the lymphatic vessels do not efficiently pump the fluid back to the blood vessels, fluid accumulates in the interstitial space, leading to swelling (also called lymphedema) and inhibiting further flow, again leading to necrosis [3]. Therefore, tissue fluid balance is necessary for healthy tissue. Aside from helping deliver large molecules to interstitial cells, IF is known to play a role in maintaining immunity and tolerance, carrying antigens present in the interstitium to immune cells residing in the lymph nodes via the lymphatic vessels for constant sampling by lymphocytes [38]. Furthermore, IF can promote chemotaxis by skewing autocrine chemokine gradients [10], which allows tumor cells to migrate to lymphatic vessels and may increase metastasis (Fig. 2) [34]. IF is increased in injured and inflamed tissue due to vessel hyperpermeability, and this increase in flow promotes fibroblast differentiation into myofibroblasts as well as cell and matrix alignment, favoring fibrogenesis [23]. IF also acts as a stimulator for lymphangiogenesis [33] [16] by helping organize microvessels [35] [37]. Flow also serves as a directionality cue, inducing morphogen gradients around cells, leading to growth in the direction of flow [14]. Finally, *in vivo* studies have shown that flow is necessary for lymphatic vessel organization [4] [31].

Since IF has a direct impact on numerous cell processes, studying any one of them *in vitro* without controlling fluid flow would be incomplete. Carrying flow is the *raison d'être* for a vessel and indeed it was shown that flow is necessary to obtain capillary-like structures containing lumen [22]. Also, as mentioned above, flow will transport morphogens and thereby influence their bioavailability. Therefore, including flow is necessary and of particular importance to angio- and lymphangiogenesis assays.

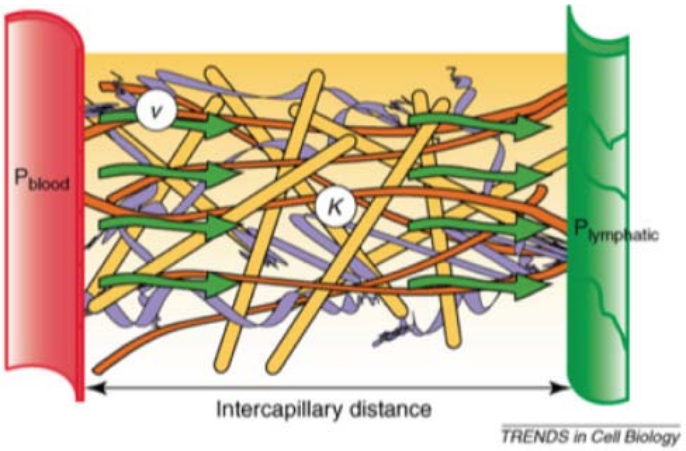

Figure 1: Interstitial fluid flows from the blood vessels to the interstitium and is drained by the lymphatic vessels. The driving force is pressure gradients [32].

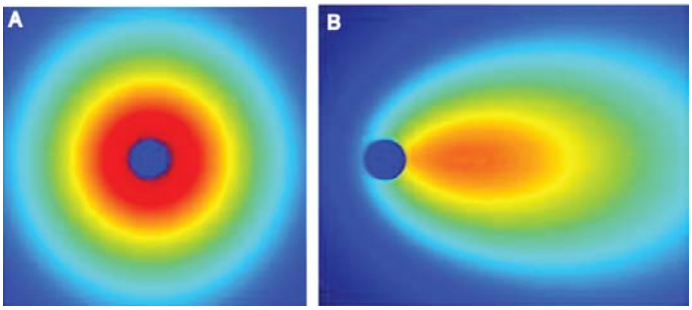

Figure 2: Flow creates an autologous chemokine gradient. **A**: gradient is distributed homogeneously around cell in static conditions, while **B**: under flow conditions, the gradient is skewed in the direction of flow [10].

There is a need to develop flow devices, and several groups have been working on this in the past decade. While each IF device will vary depending on the scientific question under investigation, several features are omnipresent: (1) small size to reduce diffusion limitations in the gel, (2) good control over pressure gradients, (3) live imaging at a viewing angle perpendicular to flow rather than parallel, since cells often grow parallel to flow, and (4) gel isolation for post-experimental analysis (e.g., PCR, flow cytometry). Most of these features exist in 3D fluidic devices used currently [42] [24] [41] [13]. However, the available systems are usually designed for a particular experiment and adapt poorly to other questions or even cell types. Finally, they present single chambers rather than a system containing multiple identical chambers. Side-by-side studies of different conditions are difficult as changes might be due to the setup rather than the experiment.

Here we implemented two systems that allow cell culture in a 3D environment under IF conditions, mimicking the tissue microenvironment to study cell-cell, cell-matrix and cell-flow behavior *in vitro*. While our 9-chamber radial flow system (9-CRFS) is versatile and can be used for many of the implications of IF mentioned previously, we chose to validate it by testing lymphatic endothelial cell (LEC) morphogenesis and lymphangiogenesis. A multi-chamber migration assay (multi-CMA) was developed as part of a European consortium aiming at developing "angiogenesis-inducing bioactive and bioresponsive scaffolds in tissue engineering" (Angioscaff, cordis.europa.edu). This system contains several repeats of two adjacent chambers to study cell migration into biomaterials developed by collaborating laboratories. In angiogenesis assays, it is particularly relevant to compare multiple conditions at the same time, such as different growth factors or inhibitors. In this thesis, we present (a) the design of our two systems along with quantification of their flow profiles, (b) a proof-of-concept study of the 9-CRFS showing capillary morphogenesis, and (c) applications of our versatile systems to other biological systems, including fibroblast and tumor cell co-culture. The work done with the 9-CRFS is to be submitted to Biotechnology and Bioengineering [5].

3 Methods and Materials

3.1 Design and fabrication of multi-chamber IF systems

Two multi-chamber interstitial flow systems were designed (Fig. 3): the 9-CRFS was based on an existing single-chamber radial flow system [25] (Fig. 4B) to study cell organization, while the multi-CMA was developed to study cell migration into biomaterials. They both consist of several identical chambers and two media reservoirs, one serving as the inlet and the other as the outlet for all chambers (Fig. 4, Fig. 5). A polydimethylsiloxane (PDMS) structure defines the compartments of the system and is closed by a glass coverslip, allowing visualization of the gels. PDMS was chosen for its inertness and documented biocompatibility as well as its good optical transparency, allowing for easy filling and imaging. The driving force for flow is the difference in pressure between the inlet and outlet reservoirs, which creates a pressure gradient across the gel. Molds, containing the negative features of the systems, were micromachined out of polymethylmethacrylate (PMMA). PDMS was made by mixing the base and curing agent (Dow Corning, 184 Sylgard base and curing agent) and injected into the mold and polymerized at 90°C for 1h30. Porous polyethylene (PE) rings, with an inner radius of 2.95 mm and an outer radius of 4.05 mm, were laser cut out of a 0.0625 inch thick sheet of PE (Small Parts PEH-060/90, Miramar, FL, USA).

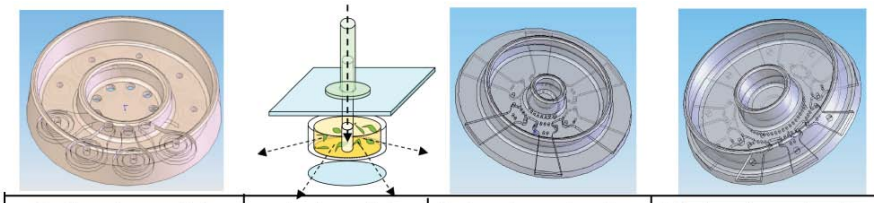

	9-chamber radial flow system (9-CRFS)	single radial flow chamber	6-chamber migration assay (6-CMA)	10-chamber migration assay (10-CMA)
Use	Cell organization Co-culture Cell invasion	Cell organization Co-culture	Cell organization Co-culture Cell invasion Cell migration into different gel	Cell organization Co-culture Cell invasion Cell migration into different gel
# chambers	9	1	6	10
Volume	540 µl	400 µl	cells: 160 µl biomaterial: 120 µl	cells: 300 µl biomaterial: 200 µl
Max. flow	2.5 µm/s	15 µm/s	3 µm/s	3 µm/s (theoretical)

Figure 3: Interstitial flow systems.

3.1.1 The 9-chamber radial flow system (9-CRFS)

The 9-CRFS consists of nine identical chambers (Fig. 4A). In these chambers, hydrophilic PE rings are inserted between the PDMS and glass to constrain the cell-containing gels and prevent matrix contraction by the cells. The inlet of each chamber is centered in the circular PE ring, leading to the same pressure gradient across all gels and to a homogeneous radial flow in all direction, which decreases with increasing radius.

3.1.2 The multi-chamber migration assays (multi-CMA)

A prototype 6-CMA was developed, followed by an optimized 10-CMA (Fig. 5). Here, the use of PE was not appropriate, as it would prevent cells from migrating from one gel to the other. Instead, to confine the gel to one compartment during filling, pillars are placed between the chambers. The geometry of the system (pillars: $\varnothing = 500\mu$m, h = 800μm in height; filling ports: $\varnothing = 800\mu$m) led to a greater surface tension between the pillars than through the filling ports, so that the injected gel fills the entire chamber before leaking past the PDMS pillars. The inlet is at the center of the system, leading to a homogeneous flow in all directions, but in contrast to the 9-CRFS, the flow is approximately uniform.

3.2 Assembly

For both systems, the inlet and outlet of each chamber were drilled in the PDMS. This allows us to choose the number of chambers used for a given experiment and prevents from having to use them all each time. Before assembling the chambers, the PDMS units and the PE rings (when used) were autoclaved. The glass coverslips (50 mm diameter, thickness #1, VWR, Dietikon Switzerland) were cleaned first with soap, then ethanol and finally acetone. The system is assembled under sterile conditions. For the 9-CRFS, PE rings are inserted into the chambers that will be used and the system is closed using the glass coverslip (Fig. 6). For the multi-CMA, the coverslip is set on the bottom of the PDMS unit. PDMS is hydrophobic, but can be temporarily rendered more hydrophilic to improve the system's surface treatment and filling properties (described below). This is done by oxygen plasma treatment (200W, 0.3 Torr, 60 seconds; Branson/IPC, Series 2000 Plasma processing reactor center) and this step further cleans the system. Plasma treatment also allows the PDMS to bond to the glass and prevents leaking between chambers or from the system. Once treated, the PDMS structure and the glass coverslip are pressed together. The chambers are then surface treated to facilitate surface bonding with the gel. First poly-L-lysine (0.01%, Sigma, Steinheim, Germany) is pipetted into each chamber for 25 minutes followed by 0.1% gluteraldehyde (Fulka, Buchs, Switzerland) for 20 minutes. Once

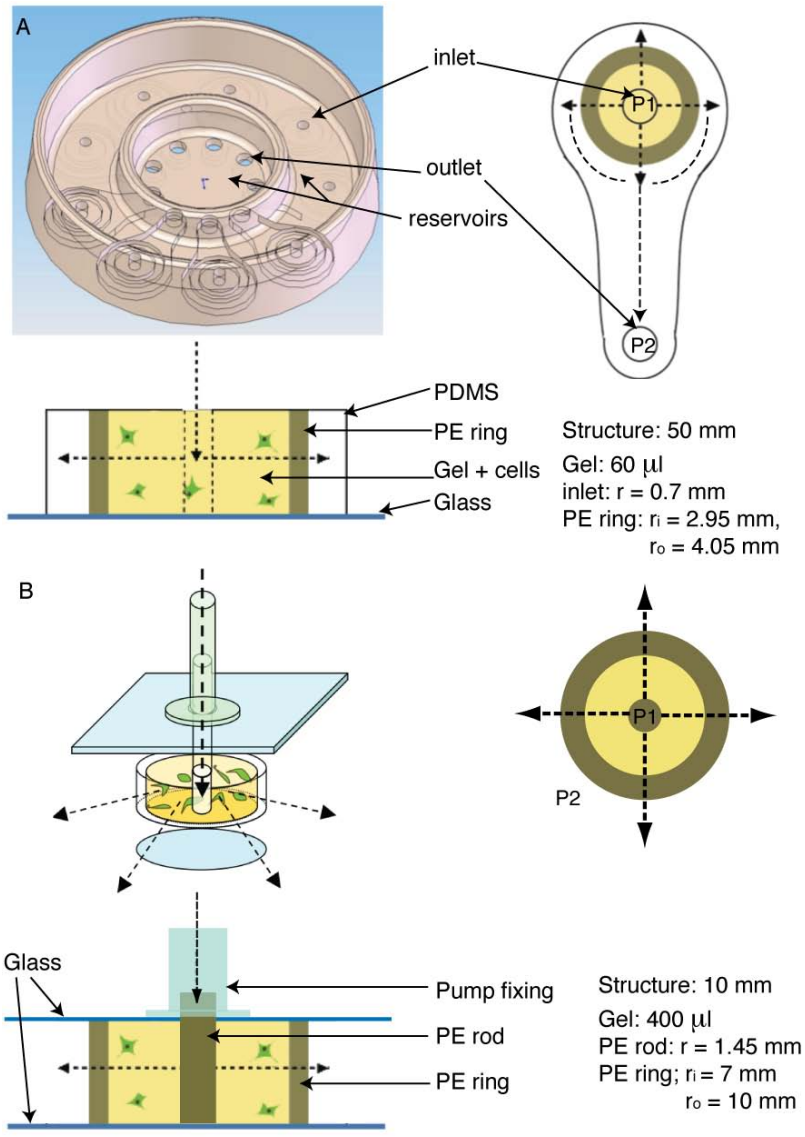

Figure 4: Radial flow systems, and top and side views. **A**: The 9-chamber radial flow system consists of nine identical chambers that feed from a common inlet reservoir and flow into a common outlet reservoir. **B**: Single-chamber radial flow system. Arrows indicate flow path.

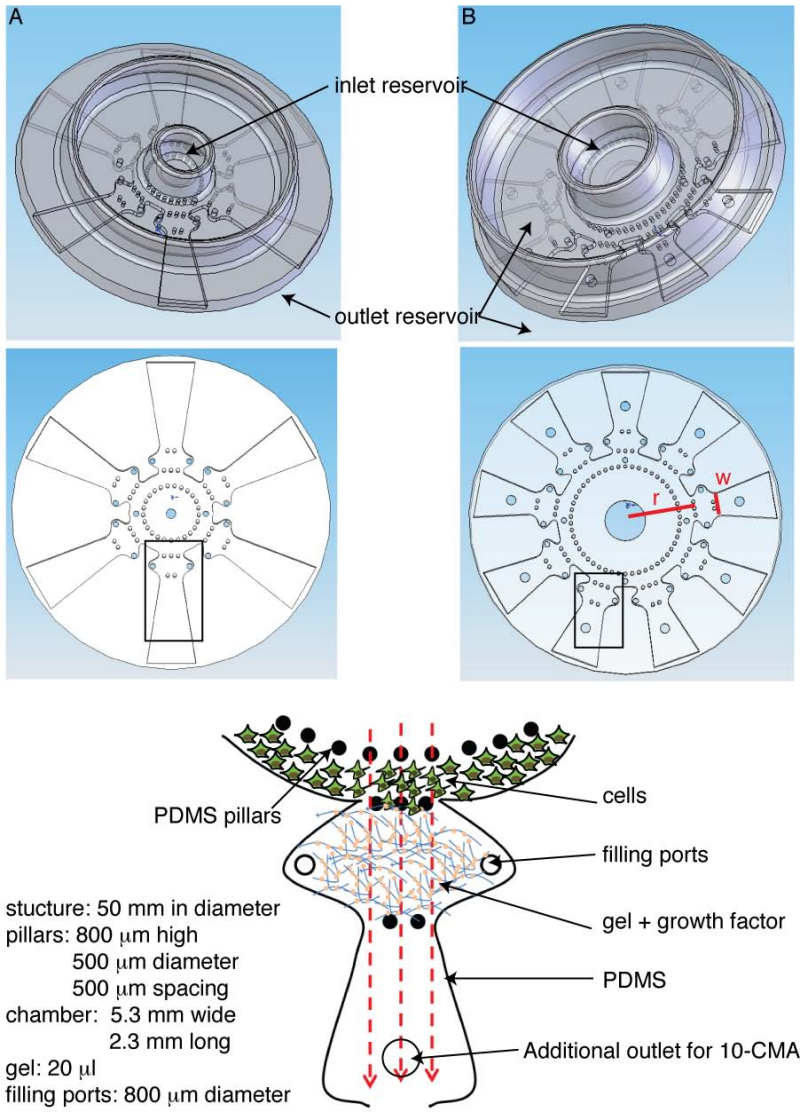

Figure 5: Multi-chamber migration assays. **A**: 6-chamber migration assay and **B**: the revised 10-chamber migration assay. All side chambers are connected to the same cell chamber, so the same batch of cells are used in all experiments. All chambers share a common inlet reservoir as well as a common outlet reservoir. Path of flow is indicated by arrows.

treated, the assembled system is rinsed thoroughly with ultrapure water and stored at 4°C for up to 3 days with all chambers filled with water to prevent drying. The effect of the plasma treatment is reversible, allowing us to disassemble the system once the experiment is done or to extract the gel. This is done by pulling the PDMS off from the glass. The PDMS structure was rinsed with ethanol after removing all remaining parts (PE rings when used, residual gel, glass, etc.) and autoclaved before reuse. It is therefore not necessary to recast new structures for every experiment, which significantly reduces the time and material used.

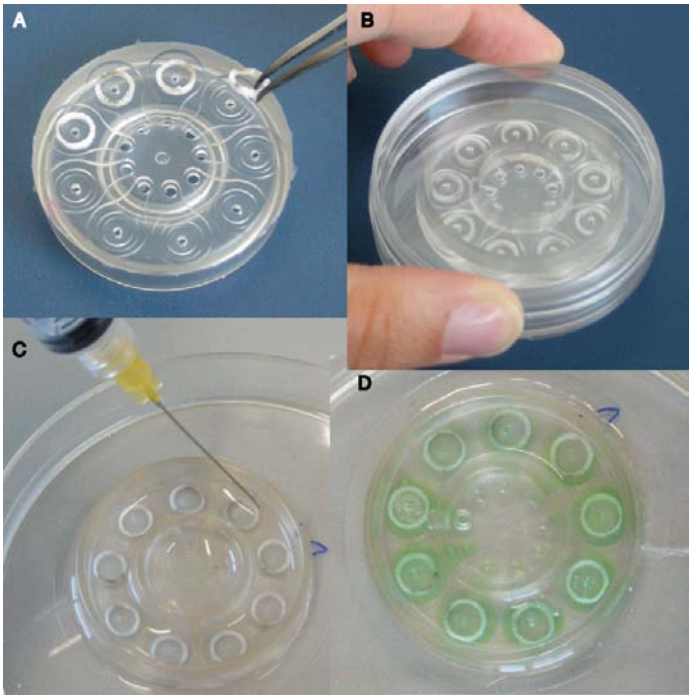

Figure 6: System's assembly. After autoclaving, the PE rings are places in the corresponding grooves in the PDMS structure (A). After closing the system with a cleaned glass coverslip, the system is pressed onto the glass using a small Petri dish (B) and forceps for the smaller regions. This step is repeated after plasma treatment to ensure proper PDMS-glass bonding. The chambers are filled with gel and the reservoirs are filled with media. Air bubbles are removed from the system using a high gage needle (C). Once the system is properly assembled, flow can be initiated and no leaking occures (D).

3.3 Characterizing flow profiles using *F*luorescence *R*ecovery *A*fter *P*hotobleaching (FRAP)

When exposed to light for too long, fluorescent molecules are damaged and lose their fluorescence permanently, a phenomenon called photobleaching. We used Fluorescence Recovery After Photobleaching (FRAP) to determine flow rates through the gel. FRAP was originally developed by Peters et al. [28] and Axelrod et al. [1]. Further improvements were made in the following decades [20], including use for flow measurements and quantification [2]. The goal was to determine the range of flow velocities that can be obtained in our systems, to test if the flow profile is consistent with the predictions given the geometry of the systems, and to check for homogeneity within a chamber and between the chambers. We can also obtain the hydraulic conductivity of our gels and compare it to published values for collagen.

A region of interest is bleached using repeated scanning by laser. In static conditions, imaging of the spot after bleaching reveals that the spot will disappear due to diffusion of fluorescent molecules into the spot. Under flow conditions, diffusion is also noticeable but convection dominates as the spot translates along with the flowing fluid (Fig. 7). The velocity of the translation correlates with the velocity of the fluid if the diffusing molecule does not interact with the gel. Either flow system was placed in a glass bottom Petri dish (to minimize the working distance as well as increase the optical transmission) and the collagen gel was perfused with a 100 μg/ml solution of 40kDa FITC-conjugated dextran (*F*luorescein *I*so*t*hio*c*yanate, Sigma) such that the entire gel contained fluorescent dextran. To determine the flow velocities throughout the chamber and to verify our predictions (see sections 3.3.1 and 3.3.2), we took several measurements at different positions in the gel. The bleached spot was a 90 μm circle in diameter in the center of the field of view. Once selected, it was bleached 100 times with a 488 nm argon krypton laser, using an inverted Zeiss LSM 510 Meta confocal microscope. Using fast Fourier transform to eliminate the effects of diffusion, analysis was performed using a custom made Matlab code (MathWorks, MA) to obtain the flow velocity [2].

3.3.1 9-chamber radial flow system

To determine the flow velocities throughout the chambers and to verify our predictions, we took five equally spaced measurements along four orthogonal radii in the chamber. Given the radial geometry of the chamber and Darcy's law, it follows that

$$\frac{Q}{A} = -\frac{K'}{\mu}\nabla P = -\frac{K'}{\mu}\frac{dP}{dr} \tag{1}$$

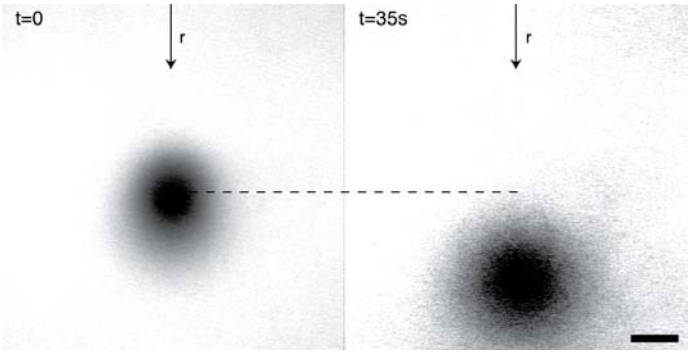

Figure 7: Fluorescence Recovery After Photobleaching. At time t=0 after bleaching, a clear bleached spot appears, which translates with flow after 35 seconds. Here since the inlet is located above the image and the PE ring and outlet are below it, flow should be in the downward direction. The bleached region moved towards the bottom of the image. Scale bar: 100 μm.

where K' is the hydraulic conductivity of the gel, μ the viscosity of the media and $A = 2\pi rh$. Integration over the radius r gives us

$$Q = -\frac{2\pi h}{\mu ln(\check{r})} K' \Delta P \tag{2}$$

where $\Delta P = P_{outlet} - P_{inlet}$ and $\check{r} = \frac{r_{outlet}}{r_{inlet}}$. By plotting Q as a function of ΔP, we obtain K', which is the slope of the fitted curve. However, FRAP does not reveal Q but v, which is related to Q by

$$v = \frac{Q}{2\pi h} \frac{1}{r} \tag{3}$$

for a given ΔP. By plotting v as a function of r, we obtain $Q = f(\Delta P)$ and thus K'. From these equations and the radial geometry, we expect the velocity to decrease as the radius increases. Also, since all chambers are exposed to the same pressure gradient and the inlet is centered in the circular PE ring, we expect the velocity to be uniform along the four axes and consistent between different chambers of a same system.

3.3.2 Multi-chamber migration assay

The individual chambers of this system are also distributed radially around the inlet. However, the radius of curvature is relatively large compared to the width of the biomaterial chamber, so it is approximately rectangular. Therefore, the assumption can be made that

flow through the chamber is linear. Using this assumption together with Darcy's law, we obtain

$$\frac{Q}{A} = -\frac{K'}{\mu}\nabla P = -\frac{K'}{\mu}\frac{dP}{dy} \tag{4}$$

with y being along the length of the chamber (Fig. 8), since there is only a significant pressure drop in this direction. Here we have $A = wh = A(y)$, where w is the width of the chamber and h its height. Integration over y gives

$$Q = -\frac{wh}{\mu}K'\frac{\Delta P}{\Delta y} \tag{5}$$

where $\Delta P = P_{outlet} - P_{inlet}$. In this case, v is related to Q by

$$v = \frac{Q}{A(y)} \tag{6}$$

for a given ΔP. Once again, by plotting v as a function of y we can extract K'. h is constant but w varies slightly, increasing up to $\frac{y}{2}$ and then decreasing again. Hence, we expect the velocity to be constant along x but vary along y (Fig. 8).

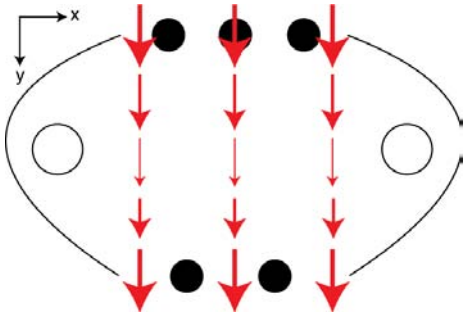

Figure 8: Expected flow profile in the multi-CMA. Thickness of arrow indicates intensity of flow, which decreases until the middle of the chamber, $\frac{y}{2}$, then increases again. Black circles indicate the PDMS pillars, empty circles are the filling ports.

3.4 Cell lines

All cell lines used in this study had been previously isolated and generated, as described below.

3.4.1 Isolation of LEC and BEC

Human LECs and blood endothelial cells (BECs) were previously isolated from neonatal foreskins using a LYVE-1 antibody [29]. Cells were expanded in collagen-coated flasks in EBM (Lonza, Basel, Switzerland) supplemented with 20% fetal bovine serum (FBS, Gibco, Invitrogen, Basel, Switzerland), 1% penicillin-streptomycin-amphotericin B (PSA, Invitrogen), 50 μM DBcAMP, 1μg/ml hydrocortisone acetate (all from Sigma) and 20 μM L-glutamine (Gibco) and cultured in a 5% CO_2, 37°C incubator. They were used at passages 6-8.

3.4.2 Isolation and generation of three fibroblast cell lines: HDF, 3T3 GFP and 3T3 lox, as well as a fluorescent tumor cell line (MDA)

Human dermal fibroblasts (HDF) were co-isolated from foreskins used for LEC and BEC cell isolation. They were labeled with a cell-permeable red dye, cell tracker red (Invitrogen). NIH 3T3 murine fibroblasts were transduced with pLV rtTAs-M2 IRES Neo lentivirus to express a tetracyclin sensitive transactivator. In order to generate a cell line expressing GFP upon exposure to doxycycline, some cells were transduced with pLV puro Tet IRES EGFP, while other cells were transduced with pLV puro Tet loxMyc4 to secrete lysyl oxidase (lox) upon addition of doxycycline. Fibroblasts were expanded in DMEM high glucose (PAA, Pasching, Austria) supplemented with 10% FBS and 1% PS. Transduced 3T3 cells were kindly provided by Dr. Valerie Weaver (University of California San Francisco, CA). MDA-MB-435S human melanoma cells (MDA) [6] were transfected with a pcDNA3.1/EGFP construct, selected using media supplemented with 600μg/ml zeocin and 400 μg/ml geneticin and expanded in DMEM high glucose supplemented with 10% FBS, 1% PSA. Transfected MDAs were a kind gift of Dr. Mihaela Skobe (Mt. Sinai School of Medicine, NY).

3.4.3 Generation of TRC wt and TRC 21+ cell lines, and F1 and F10 GFP tumor cell (TC) lines

Lymph node T-cell area-associated reticular cells (TRCs) were previously isolated from peripheral lymph nodes of p53 -/- mice and clones were selected by serial dilutions in order to generate an immortalized TRC cell line [40]. TRC cells were transduced with a pgk-Tomato lentivirus in order to express a red-orange fluorescent protein and expanded in RPMI 1640 (Gibco) supplemented with Glutamax (Gibco), 10% FBS, 1% PSA, HEPES (12nM, Gibco) and β-mercaptoethanol (50μM, Sigma Aldrich). In order to generate a TRC cell line that over-expresses the secondary lymphoid tissue chemokine CCL21 (TRC 21+) compared to the wild type cells (TRC wt) that express very low levels of autologous

CCL21, some cells were transduced with a pgk-CCL21 lentiviral vector produced from cDNA of murine CCL21, kindly provided by Dr. Didier Trono (EPFL, Lausanne). Murine B16 F1 low metastatic and B6 F10 (ATCC, Middlesex, UK) high metastatic melanoma cells were transduced with pgk-GFP lentiviral vector and expanded in DMEM high glucose supplemented with 10% FBS and 1% PSA.

3.5 Matrix preparation and filling

For the 9-CRFS, 40 μl of gel was pipetted into each chamber and allowed to polymerize at 37°C for 20 minutes. When performing a co-culture experiment, both cell types were mixed together in the gel preparation and seeded simultaneously. For the multi-CMA, 160-300 μl of gel containing cells is pipetted into the central compartment, followed by 20 μl of gel without cells into the each side chamber. As above, the gel was allowed to polymerize for 20 minutes before adding media to all reservoirs for static conditions that were maintained for at least 12h, allowing cells to adjust to their new environment. To initiate flow, media was removed from the oulet reservoir, creating a pressure gradient across the gel, and this step is repeated once daily. It is important to remove all air bubbles that might be trapped at the inlets, outlets or within the path of the fluid before this step (especially for the 9-CRFS), as the presence of an air bubble will prevent fluid flow. Different cell types were used for different experiments. A summary is given next (Fig. 9).

	LEC and BEC	MDA and fibroblast	MDA migration	B16 and TRC	FRAP
System	9-CRFS	9-CRFS	6-CMA	9-CRFS	both
Goal	capillary formation	Changes in matrix	Migration from one gel to another	B16 invasion TRC networking	Flow quantification
Matrix	fibrin	collagen	collagen	collagen	collagen
Density	1.5-3 million	MDA: 0.5 million Fibroblast: 0.25 milion	0.5 million	B16 2.8 million TRC 1 million	-

Figure 9: Different cell types are used depending on the experiment.

3.5.1 Lymphangiogenesis assay

LECs and BECs were cultured in fibrin gels. The fibrin gel was prepared by combining 3 mg/ml human fibrinogen (Sigma), 2 U/ml factor XIII (Baxter, Deerfield, IL), 200 U/ml

aprotinin (Sigma), 2 U/ml human thrombin (Sigma), 2 mM $CaCl_2$ (Fisher, Fairlawn, NJ) and TBS, and 100 ng/ml TG-VEGF (when used). Cells were seeded at a density of 1.5 x 10^6 cells/ml or 3 x 10^6 cells/ml. The recombinant fibrin-binding TG-VEGF was used as described previously [45] [15]. This matrix-binding growth factor covalently cross-links into fibrin by factor XIII, preventing its rapid diffusion compared to wild-type VEGF, but it can be released by enzymes secreted by cells [45].

3.5.2 Tumor-fibroblast co-culture

A 1.8 mg/ml collagen gel was prepared according to the manufacturer's recommendations using rat tail type I collagen (BD, Basel, Switzerland), supplemented with 0.01M HEPES and 5% Matrigel (BD). MDAs were seeded at 500'000 cells/ml, and fibroblasts (HDFs and 3T3s) at 250'000 cells/ml.

3.5.3 Tumor in lymph node

TRC cells were resuspended into 2.25 mg/ml type I collagen and 10% Matrigel. TRCs were homogeneously seeded in the gel mix at a density of 10^6 cells/ml and injected into the chambers and before the matrix polymerized, a thin sterile rod was inserted into the inlet to create a cylindrical hole that is the same for all the conditions. After polymerization (10-15 minutes), the rod was withdrawn and 5 μl of gel containing B16 cells at a high density (2.8 x 10^6 cells/ml) was injected to mimick a tumor mass. The gel was left to polymerize another 20 minutes before media was added.

3.5.4 FRAP

We used 1.8 mg/ml collagen gels without Matrigel for flow quantification experiments (see section 3.3).

3.6 Staining and imaging cell structures

Imaging through the glass coverslip is perpendicular to the direction of flow, which is optimal to observe cell structure and organization. The cells were stained for actin fibers with Alexa Fluor 488 phalloidin (Invitrogen) and nuclei with DAPI (4'-6-*d*iamidino-2-*p*henylindole, Invitrogen). The cells were fixed using 2% paraformaldehyde (PFA, Fluka, Sigma-Aldrich) by filling the reservoirs for 1h at 4°C and then stained overnight at 4°C with 5 U/ml phalloidin. The gels were imaged on an inverted white light laser confocal

microscope (Leica SP5) and 2D projections of the 3D stacks were generated that were further processed using ImageJ (NIH public-domain image processing software). To visualize lumen formation, confocal reflectance microscopy was used. A slice was analyzed using Imaris software (Bitplane, Zurich, Switzerland). Bright-field images were taken using an inverted fluorescent microscope (Zeiss Axiovert 200M, Switzerland) with a CCD camera (AxioCam MRm). This was used to image a whole chamber as well as to determine viability of cells by time-lapse imaging and checking for cell motion. For time-lapse imaging, the chamber was mounted onto the stage of the microscope and images were taken every 6 minutes for 3 hours. To determine cell migration, images were always taken in the same plane (middle of the gel height).

4 Results

4.1 The 9-chamber radial flow system

4.1.1 Design of the 9-chamber radial flow system

A fluidic system was designed for side-by-side comparison of simultaneous cell cultures under different conditions while ensuring that differences in cellular behavior are due to the microenvironment selected and not to the chamber properties. Our system consists of nine chambers created in a single PDMS unit, that are all exposed to the same pressure gradients, thus leading to a similar flow velocity in each case, provided the resistance is the same in each gel. The design was based on a previously developed radial flow chamber [25]. Our system is 5 cm in diameter and fits nine smaller versions of the single-chamber system, which can be placed in a traditional Petri dish and mounted on a microscope stage. The smaller chamber now holds 40 μl of gel instead of 400 μl, thereby significantly reducing the amount of reagents and the number of cells used. The materials were chosen for their known biocompatibility. PDMS was chosen for the ease of molding as well as its good optical transparency, which facilitates filling, handling and imaging. The glass coverslip used to close the system permits conventional transmission, epifluorescence, and confocal microscopy. The PE rings are important for confining the gel to a delimited region and necessary to prevent gel contraction by contractile cells, such as fibroblasts [18]. The hydraulic conductivity of PE is greater than that of fibrin or collagen gels, which means the PE ring does not change the flow profile within the gel. Given the radial geometry of the chamber, the flow velocity is expected to be higher at the center of the chamber (near the inlet) and decrease with increasing radius. Thanks to this characteristic, the effect of several flow velocities can be determined within a single chamber. A challenge is preventing leaking. One of the options involves using glue, but glue contains substances toxic to cells, which could affect their viability. Silicon sealant is another option, but this makes dismantling of the chamber for reuse or gel extraction difficult. However, by pressing the PDMS structure and the glass coverslip firmly immediately after plasma treatment, using forceps for the small surfaces, we were able to ensure a firm seal. Another challenge is pipetting the gel into the chambers while avoiding air bubbles, which can alter the flow profile or cause leaking. By holding the pipet vertically with the tip mid-distance between the inlet and the coverslip and leaving the system horizontally in the hood, these were avoided. Moreover, if problems did occur during filling, the gel can be aspirated out and filled again.

4.1.2 Flow profile

The radial geometry of the chambers, along with Darcy's law, let us predict that the flow velocity within the gel should decrease as we move towards a larger radius. This was confirmed quantitatively with FRAP. The flow velocities were determined using a custom made Matlab script; the expected profile was verified and found uniform along all axes and consistent between chambers (Fig. 10A). Further analysis revealed that the velocity increases with increasing pressure heads, and that the flow rate increases linearly with pressure (Fig. 10B). From the slope of the linear regression, the hydraulic conductivity of the collagen gel was determined to be $K' = 5$ x $10^{-10} cm^2$, which is within the expected range of 0.16 - 3 x $10^{-9} cm^2$ for collagen [25]. These data were taken from a representative chamber in the system.

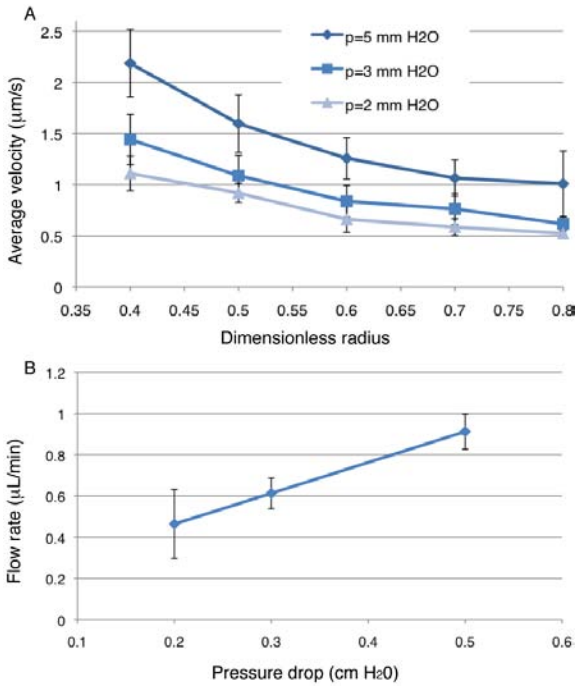

Figure 10: Characterization of interstitial flow within a culturing chamber. FRAP is carried out in a chamber to characterize the interstitial flow. **A**: The average velocity within the chambers decreases as the radius increases, as expected from the radial geometry of the chambers. The velocity increases with pressure. Position and pressure drop have a significant influence on flow velocity ($p < 0.5$ using anova). **B**: The flow increases linearly as a function of the pressure head as predicted from Darcy's law. The slope represents the hydraulic conductivity K', which in this case is 5 x 10^{-10} cm^2.

4.1.3 Cell survival and morphology

Cells survived and grew in the chambers during the five- or ten-day experiments, showing biocompatibility of the chamber. In an experiment comparing a single-chamber system [25] and the 9-CRFS, LECs grew and organized in a similar manner, showing that the 9-CRFS supports cell behavior comparably to the preexisting system from which it was derived. In both cases, when cells were grown in static conditions, they remained rounded within the gel (Fig. 11A), while when exposed to flow, they spread and formed multicellular structures (Fig. 11B) containing a lumen (Fig. 11C). Time-lapse imaging was used to verify that the rounded cells were viable, and that they were rounded due to the lack of flow, not the lack of nutrients or oxygen necessary for survival (data not shown).

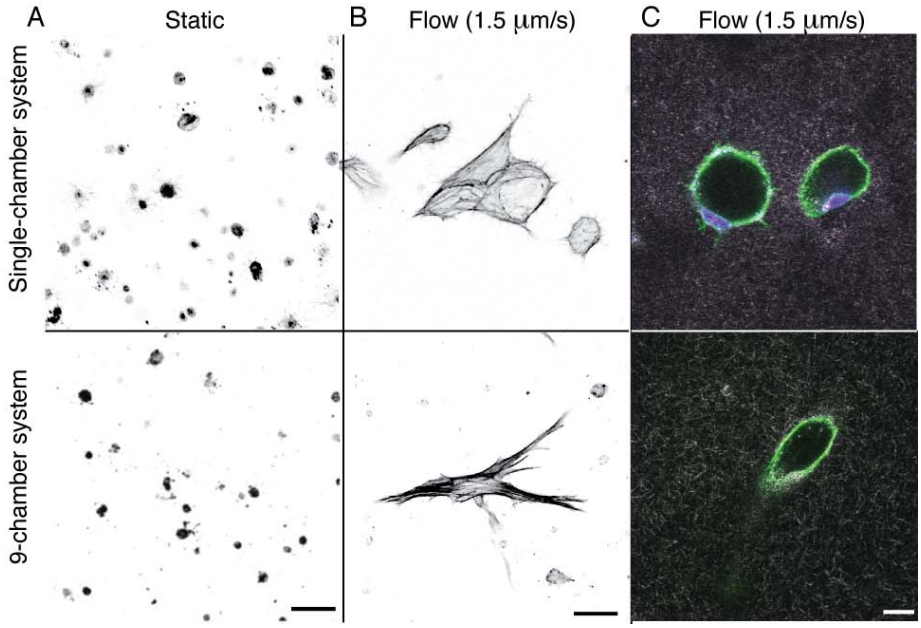

Figure 11: Comparison of lymphatic endothelial cell (LEC) response to flow in the 9-chamber system vs. the larger, single-chamber system at day 5. Confocal imaging, projection of four equal thickness (65 μm) 3D stacks. **A**: LEC remain rounded in static conditions, whereas **B**: they arrange into organized structures containing lumen when exposed to flow (**C**). The cells grow similarly in the single-chamber or the 9-chamber system. Actin stained with phalloidin, nuclei with DAPI, scale bar: A-B: 50μm, C: 15 μm.

4.1.4 Uniformity of overall cell organization

When grown under flow conditions, structures formed uniformly throughout each chamber. The density decreased when moving from the inlet towards the outlet (increasing r), but when comparing the different quadrants of a chamber or when comparing different chambers, the structure density was comparable (Fig. 12). The cells survived and organized similarly in all directions. This allows running parallel studies, knowing that all chambers perform similarly when exposed to the same culture conditions. The only variability between chambers should thus be components added to the gel, such as different growth factors or cell types. The higher organization density near the inlet could be due to the higher velocities at this location, although this was not verified in this study. Nutrients are not a limiting factor though, as structures formed throughout the chamber and time-lapse imaging showed viable cells.

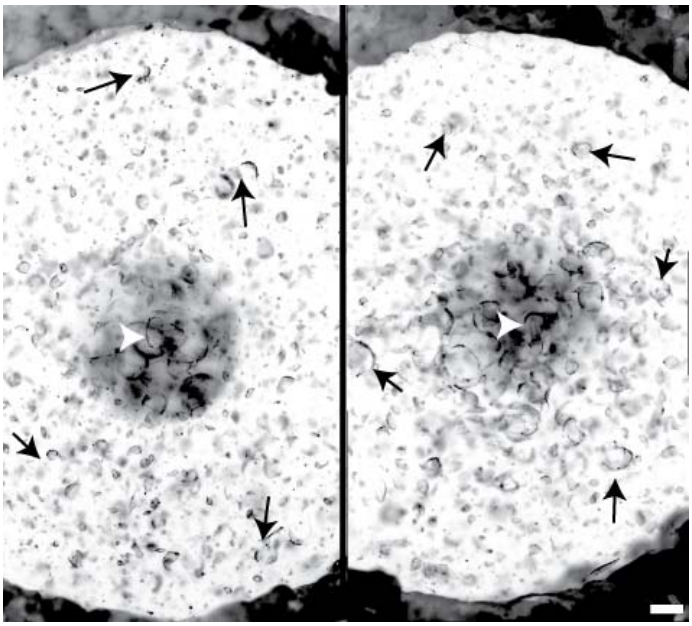

Figure 12: Uniformity of overall cell organization in the 9-chamber radial flow system. Lymphatic endothelial cells (LEC) after 5 days exposed to flow. Two chambers in a system show multicellular structures (black arrows) throughout the chamber, a little denser around inlet (white arrowhead), as well as a similar growth between the two chambers. Cell organization is homogeneous. Scale bar: 200 μm.

4.1.5 LEC and BEC morphology in the presence of VEGF

LECs and BECs show higher organization when grown in a VEGF-containing matrix. Cells were grown for ten days under flow conditions. Since all chambers were exposed to flow, cell organization was observed in all of them. When VEGF was added, the structures were more organized and denser (Fig. 13). This confirms previous data showing synergy between flow and VEGF [14]. LECs formed slender and elongated structures, while BECs were recognizable by their broad structures. In all four conditions, the structures contained lumen, indicating that flow and VEGF contribute in creating functional vessel-like structures. We chose to grow both cell types in fibrin gels even though BECs prefer a collagen environment [15] in order to only analyze differences due to cells and growth factors, not ECM.

4.2 The multi-chamber migration assay

4.2.1 Design of the multi-chamber migration assay

This system was developed to study cell migration and organization into a biomaterial, with all cells coming from the same batch. For this, two compartments are needed: one containing the cells and another containing the biomaterial. One challenge was in preventing the mixture of the two gels during filling while still allowing cells to migrate from one to the other. For this system, a PE part was not appropriate, as cells cannot migrate through it. We chose to use pillars to delimit the two compartments. The geometry we used (500 μm in diameter and 800 μm in height) resulted in a higher surface tension between the pillars than through the two filling ports in the chamber (800 μm in diameter) so the chamber is completely filled before gel starts leaking across the pillars. We also wanted this system to have several identical chambers. The 6-CMA was designed to have a small inlet to minimize the amount of cells used (since the geometry of the inlet influences the size of the cell reservoir), six identical chambers, and outlets flowing into the Petri dish, preventing media build up and thus rapid pressure gradient loss due to equilibration. This model showed several problems. The inlet reservoir was too small, requiring a pump to ensure constant presence of media. The outlet flowing into the Petri dish meant the entire dish must be filled to obtain static conditions and the system could not be placed onto a microscope without being in a dish (to prevent liquid from leaking onto the microscope), limiting the choice of microscopes as some do not have a stage for Petri dishes. This led to the 10-CMA, an optimized design based on the 6-CMA. The inlet was made bigger, which led to more cells being used, but also meant that more chambers fit on the system: we presently have 10. For the outlet, both options are available: an outlet can be drilled so that the fluid flows into a reservoir, where it will accumulate but not leak out of the system, or it can be drilled on the side of the chamber, preventing fluid accumulation. Both

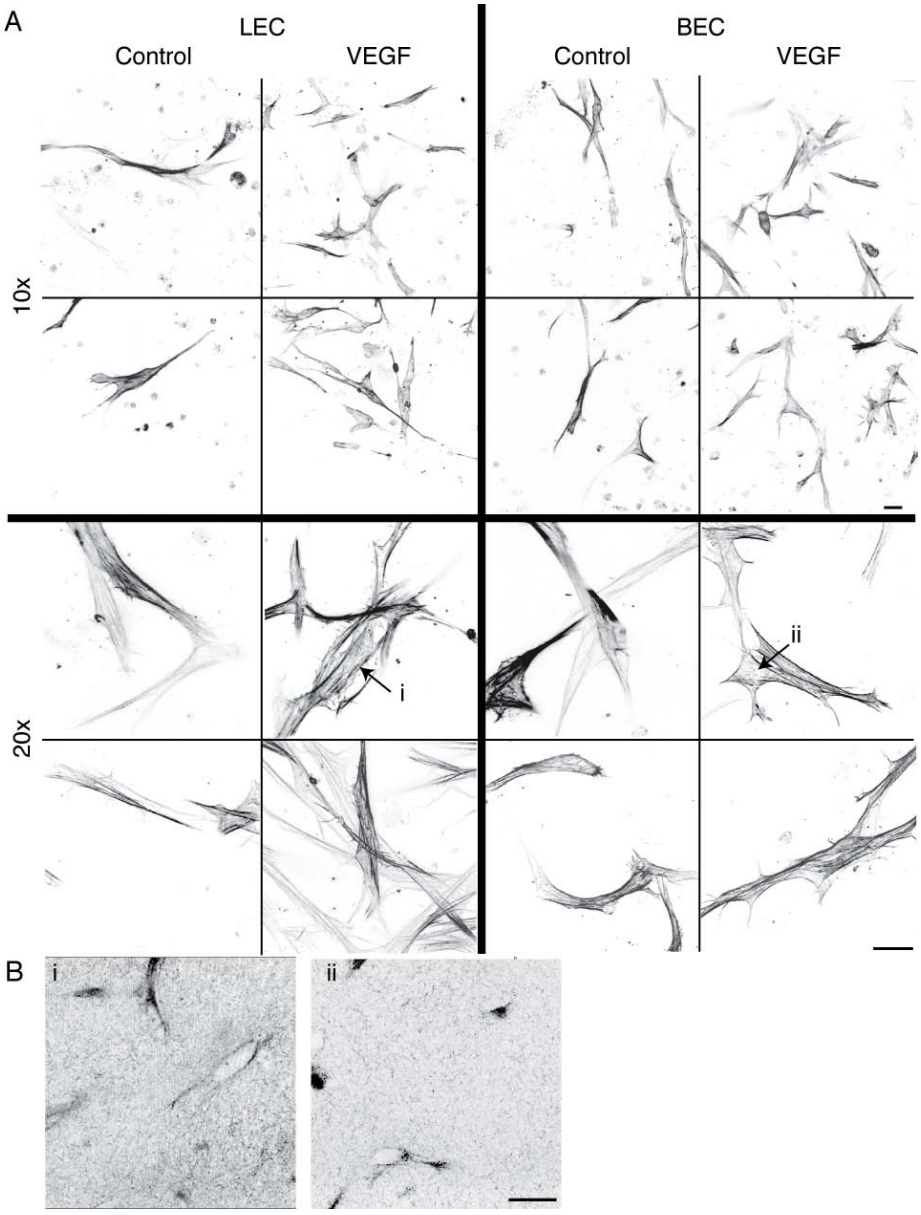

Figure 13: VEGF-A promotes organization of lymphatic and blood endothelial cell (LEC and BEC). **A**: Cells grown in the absence of VEGF formed multicellular structures, but when they were grown in the presence of VEGF, these structures were denser and the cells broader. Also, BEC show more sprouting with VEGF than without. **B**: When looking at a slice, we see that both cell types organize to form lumen, here when cultured with VEGF. All cells were grown under flow conditions. Projection of 3D stacks taken by confocal imaging, actin stained with phalloidin, scale bar: 10x: 50 μm, 20x: 20 μm.

designs require only 20 μl of gel in each chamber, minimizing the amount of biomaterial used and thereby the cost. The cell compartment is bigger though, and the first design requires about 160 μl, whereas the second one requires around 300μl. This volume might seem large, but it is similar to the 9-CRFS, which uses 360 μl for nine chambers. Once again, we used PDMS and glass for the reasons mentioned in section 4.1.1 and all chambers have the same inlet reservoir and outlet reservoir, leading to the same pressure gradient across each chamber.

4.2.2 Flow profile

For this system, we expected the flow to be linear, because even though the chambers are placed radially around the inlet, the width of the chamber is small compared to its distance from the inlet, making the assumption of linear flow through the chamber valid (w $\ll$ r in Fig. 5). This assumption was confirmed by measurements (Fig. 14). Flow is directed towards the outlet and is constant along the x axis but varies as a function of y. Once again, we show that velocity and flow rate increase linearly as pressure head increases. Measurements between the PDMS pillars might not be very representative of the chamber, since the area at this location is reduced. From these measures, the hydraulic conductivity was determined to be $K' = 1$ x $10^{-9} cm^2$, which again is within the expected range for collagen [25].

In the 10-CMA, the filling ports used to fill the chambers with the biomaterial are exposed to the outlet reservoir. Flow could thus enter through these holes, disturbing the major flow direction. Experimentally, our data show this is not the case, as the measurements close to the filling ports do not differ from the other measurements in the chamber. However, if this were a problem, these holes could be plugged using a material with a higher resistance than collagen or fibrin (such as Matrigel, agarose, agar or paraffin). This hypothesis was tested using the 6-CMA but should be identical with the 10-CMA.

4.2.3 Cell survival and homogeneity

MDAs were grown in the 6-CMA to test for cell survival. When imaged directly after seeding, the cells were rounded but after two days culture under flow conditions, MDAs spread and produced extensions (Fig. 15). Cells profilerated, as the cell density increased (Fig. 5).

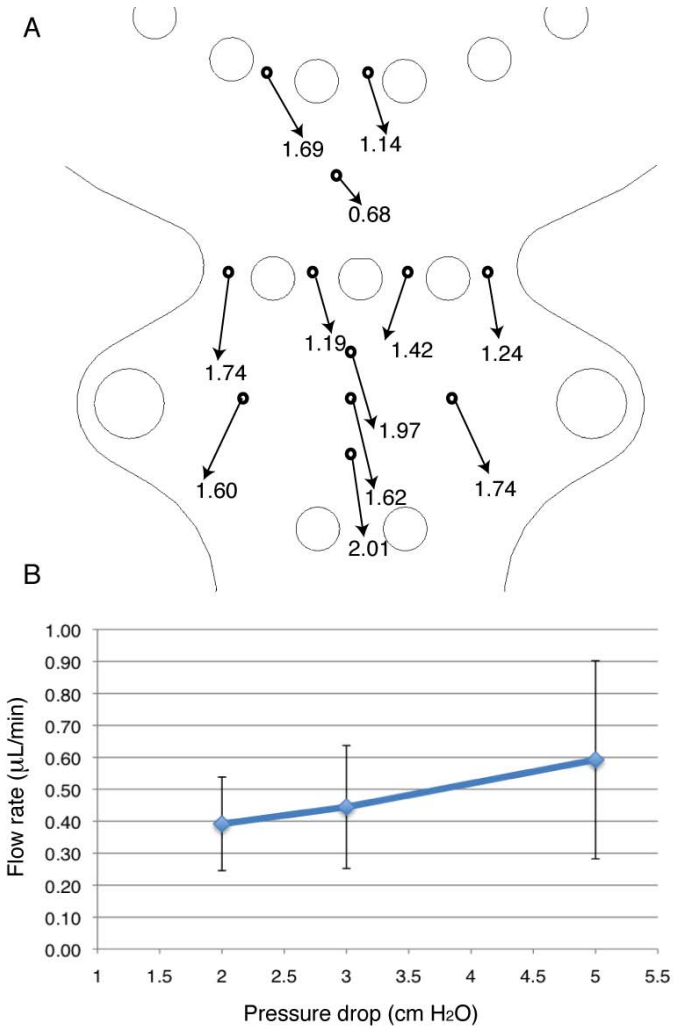

Figure 14: Characterization of flow profile in the 6-CMA using FRAP. **A**: Average velocity through a chamber. The beginning of the arrow indicates where the measurement was taken and the magnitude represents the average velocity at that point, taking into account the x and y component. The assumption that flow is linear is confirmed, as fluid moves towards the outlet. The average was taken over several measurements as well as several pressure heads. Flow velocities are given in μm/s. **B**: The flow increases linearly as a function of the pressure head as predicted from Darcy's law. The slope represents the hydraulic conductivity *K'*, which in this case is 1 x 10^{-9} cm^2.

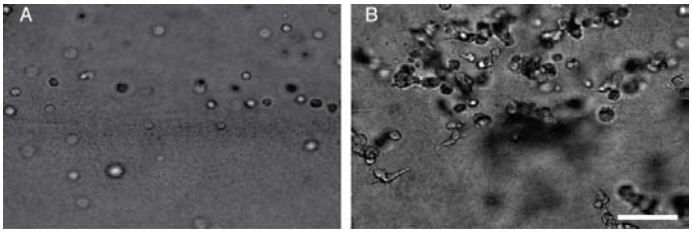

Figure 15: MDA proliferate in the 6-CMA. **A**: Directly after seeding, cells are rounded. **B**: After two days cultured in flow conditions, the cells have spread Scale bar: 100 μm.

4.3 Other applications of the 9-CRFS

Even though the 9-CRFS was mostly used for angiogenesis in this study, it is not limited to this application. As mentioned in section 2, IF promotes tumor cell migration towards lymphatic vessels through chemotaxis [10] [34]. These cells must move through the interstitium, which is made up of ECM, fibroblasts and other cell types. When tumors spread via the lymphatic vessels [19] [44], lymph node (LN) metastasis is the first step. It is thus critical to understand how TCs enter, interact and exit the lymph node (LN). The metastasis potential of TCs is strongly correlated with tumor cell expression of CCR7 receptor, which binds to the chemokines CCL19 and CCL21, allowing the cells to chemotact to the source of these chemokines [21] [39].

4.3.1 Lymph node metastasis

In order to investigate the complex interactions between TCs and LN resident stromal cells, murine melanoma B16 cells with high metastatic potential (F10) or low metastatic potential (F1) were co-cultured with wild-type (TRC wt) or CCL21 over expressing (TRC 21+) TRCs. We compared TRC co-cultured with TCs to TRC only gels and TCs co-cultured with TRCs to TCs only gels. The outcome indicators were the radius of tumor mass and TRC proliferation and networking at different time points. Cells grew under flow conditions for seven days and the interaction was imaged daily by fluorescence microscopy and at the last time point by confocal microscopy. In order to compare cell migration between different days, images were always taken in the same focus plane (middle of the gel height), to avoid the risk of comparing images taken at different focus planes in the z-axis and therefore different radii of tumor mass. For these preliminary experiments, the rod method was not used for seeding TCs. Therefore, we cannot compare the spreading of TCs into the TRCs sector, as the initial conditions varied. However, the interactions between the different cell types could be compared. When culturing TRCs alone, both TRC wt and TRC 21+ uniformly spread through the matrix after one week culture, indicating

that culture in the chamber does not affect cell viability during this time course, though TRC 21+ seem to proliferate more than TRC wt (Fig. 16). Nevertheless, in the presence of both F1 and F10, TRC 21+ appeared rounded after seven days. This might indicate cell death, though a cell viability test was not performed, or an indicator of reduced capability of TRCs to form 3D networks and interact with each other. Finally, TRC wt seemed to form a better interconnected 3D network when co-cultured in the presence of the more metastatic F10 cells, than in the presence of the less metastatic F1 cells. The purpose of these preliminary experiments was to show the versatility of the 9-CRFS. We demonstrated the feasibility of co-culturing lymph node stromal cells and tumor cells in our system, and could use this system for further studies.

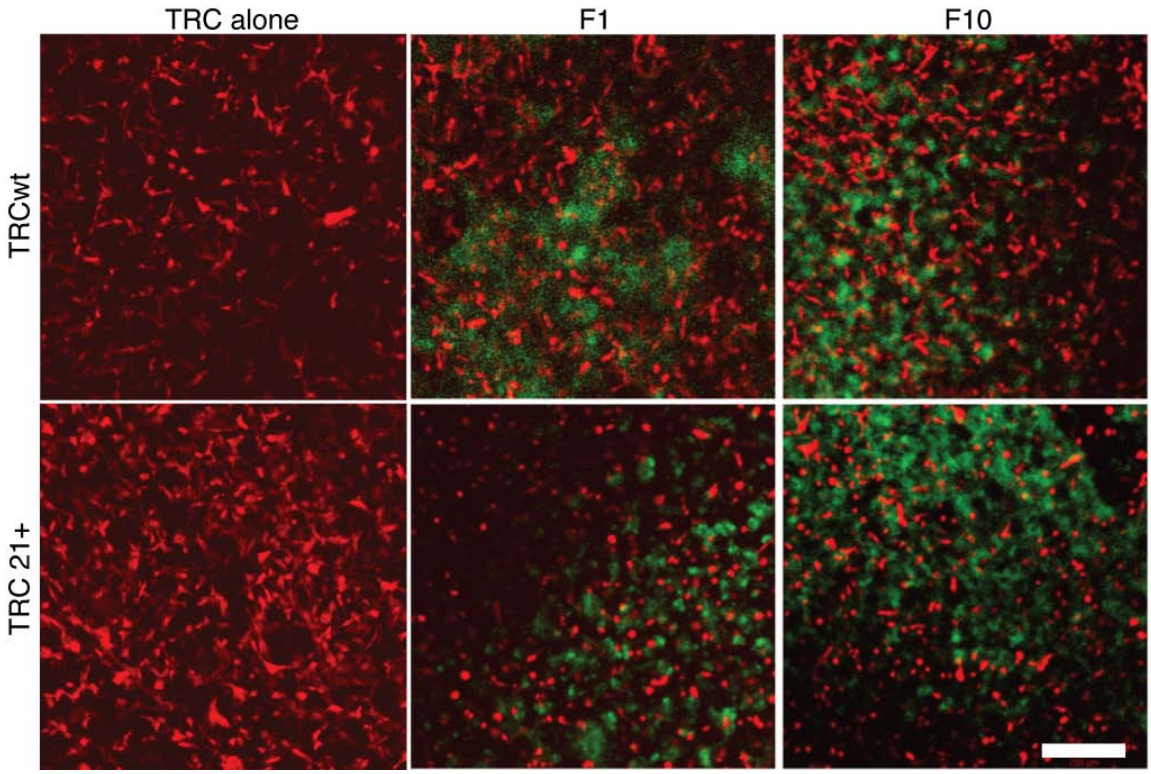

Figure 16: TRC and B16 after seven days co-culture. TRC wt and TRC 21+ cultured alone spread evenly in the matrix, though TRC 21+ seem to proliferate more. In the presence of F1 or F10, TRC 21+ appear rounded- TRC wt form a better interconnected network when cultured with F1 rather than F10. Scale bar: 200 μm.

4.3.2 Cells and flow influence the matrix

Previously, it was shown that fibroblasts align collagen fibers and differentiate when exposed to flow [23]. These changes led us to believe that the effect of flow on matrix and fibroblasts could combine and change the microenvironment in a way that would induce tumor cell migration. First, we looked at the evolution over time of the collagen matrix in the presence of MDAs, HDFs or both in co-culture, as well as in static and flow conditions. The higher density of matrix around the fibroblasts is a sign of their high contractility. Also, "bunching" of collagen fibers is visible at the end of the fibroblast projections. The most noticeable change in the matrix organization is that the matrix seems to be broken down in the presence of fibroblasts. Indeed, when culturing cancer cells alone, the fibers are long, but when culturing fibroblasts alone or in the presence of MDAs, the fibers look much shorter (Fig. 17).

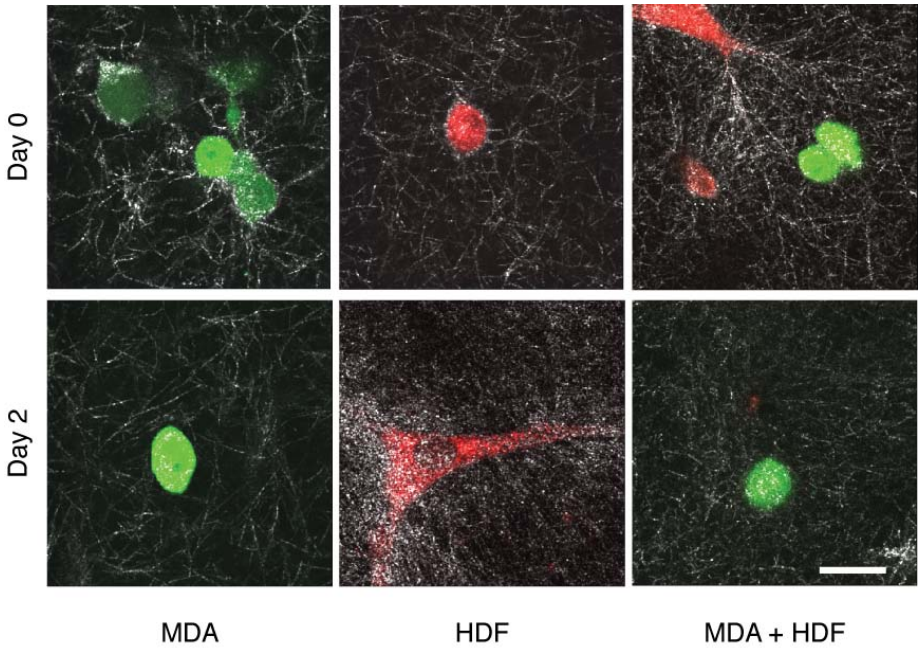

Figure 17: Collagen matrix looks different after two days flow culture with or without fibroblasts. Directly after seeding (day 0), the collagen looks similar everywhere. After two days in the presence of MDA melanoma cells, the fibers still look the same but in chambers where HDFs were grown, in co-culture with MDAs or alone, the collagen fibers look much shorter. Scale bar: 200 μm.

To further test the hypothesis that fibroblasts and flow have an effect on the matrix, the second experiment was run with two types of 3T3 fibroblasts. One of the cell types, 3T3

lox, was engineered to secrete lox upon addition of doxycycline, which cross-links collagen, making the matrix stiffer and thus presumably allowing the cells to contract more. The other cell type, 3T3 GFP expresses GFP when the same substance is added, as a control for the efficiency of doxycycline. We also used chambers containing only gel as a control. The experiment was carried out over six days under flow conditions. Directly after seeding, the gels looked all alike, but after six days of culture, slight changes are visible. The chambers containing only gel are still the same but in the ones containing fibroblasts, the matrix looks scarcer, especially in the presence of 3T3 lox, where matrix looks absent from some areas (Fig. 18). This is consistent with the results from the fibroblast-tumor cell co-culture, where the matrix appears to break down in the presence of fibroblasts: two hypotheses are that the matrix has been extensively broken down, or the fibroblasts are contracting the matrix and creating holes in the gel. When looking at the system by eye, gel contraction is not visible though.

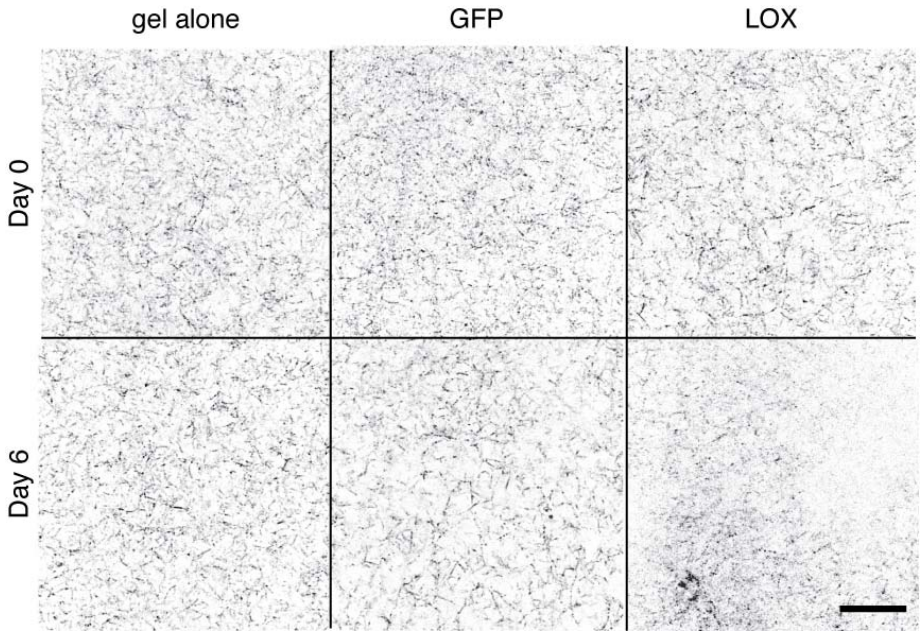

Figure 18: Effect of fibroblasts on collagen matrix. Directly after seeding (day 0), all gels look similar, but after six days under flow conditions, only the gel without any cells still looks the same: in the presence of fibroblasts, the matrix is less visible, in particular in the case of 3T3 lox. Scale bar: 200 μm.

5 Discussion

In the present work, we show two new robust systems to study cell growth, morphogenesis and migration in a 3D gel when exposed to interstitial flow and to test, side-by-side, how these are influenced by different microenvironments. This is possible thanks to multiple identical chambers, allowing up to ten different conditions within a single-chamber flow system, or replicates for fewer conditions. All desired features mentioned in the introduction were achieved: (1) by reducing the size of the chambers in the 9-CRFS, we not only reduced the amount of materials (and cells) needed, but also decreased the diffusion length. The time required for a molecule to diffuse from the inlet to the PE ring is three times lower in the 9-CRFS compared to the previous single-chamber radial flow system, and the surface area to volume ratio has increased by 2.43 times. Furthermore, given the smaller size, nine chambers can fit on a system of only 5 cm in diameter, which fits on a traditional microscope stage. The smaller size yet of the chambers in the multi-CMA means the amount of biomaterial necessary is minimal, thereby greatly reducing the cost, as the biomaterial is often very costly or difficult to synthesize, in the case of novel biomaterials. (2) The FRAP data showed flow profiles similar to what we had predicted from the two different geometries (Fig. 10 and Fig. 14). Both systems have a tunable flow, between 0.5 and 2.5 μm/s depending on the position in the chamber and the applied pressure head, which corresponds to the physiological range (0-2 μm/s [7] [17] [9]).

However, in our case the flow velocity cannot be kept exactly constant, as the pressure head will decrease as media flows through the chamber. Since a finer tuning of the flow velocity can be desired, both systems were also designed so a pump can be used. A thin tube is set in the inlet reservoir and the flow velocity is set higher than through the gel. The inlet reservoir will overflow into the outlet reservoir, from which a thicker tube will remove the excess media at a higher flow rate. The inlet reservoir will always be full and the outlet always close to empty. Different media heights can be obtained by changing the pump flow rate or fixing the tubes at a certain height in the reservoirs. A constant media height can thus be maintained, leading to a constant flow velocity. (3) The good optical transparency of PDMS and the small size of the systems are well adapted for live imaging and *in situ* fixing and staining. (4) The bond between the PDMS and the glass coverslip is reversible and the gel can be isolated for post-experimental analysis by opening the system or even pipetting some gel out through the inlet.

Furthermore, we have shown the systems' biocompatibility with cell studies. Using the 9-CRFS, we were able to confirm previous experimental results that show the effect of flow and VEGF on LECs and BECs capillary-like formation (Fig. 11 and Fig. 13), showing that our system is reliable for studying cell morphogenesis in 3D gels and that the cells are not influenced by the setup but rather by the chosen conditions. An advantage of having varying flow velocities within a chamber is that the effect of several flow velocities

on cells can be studied within a single experiment, either qualitatively by observing the cells, or quantitatively by adding FRAP measurements to know the experimental velocity at a given spot. We showed that cells proliferate in the 6-CMA, but further optimization of filling is necessary to obtain migration from a gel to the other. Increasing the pH of the biomaterial gel could be tested, as this increases the stiffness of the gel and therefore favors cell migration [8]. Once this is achieved, we will have a very powerful tool with a wide area of application in tissue engineering studies.

The mold for the 10-CMA has not been manufactured yet, but the geometry of the chambers is identical in both designs, so assembly and filling should be identical as well, and the FRAP data from the first design should be proportional to what we expect in the second. The flow profile and the dependence of pressure should remain the same. The system can also be used similarly to the 9-CRFS, where only the small chambers are used to seed cells and the bigger central compartment is left empty. The same situation as with the 9-CRFS can be obtained except the flow is constant instead of varying radially. Finally, the direction of flow can be inverted by filling the outlet reservoir more than the inlet reservoir. This could be interesting when studying processes that are believed to change depending on forward or reverse flow [36] or when studying the invasion of several cell types into a common matrix.

Given the expertise we obtained from creating these chambers and the simplicity of the setup (PDMS, PE rings, glass), it would be easy to redesign a device specifically for each question we might want to address, if it requires specific geometries. It took much less time and effort to get the multi-CMA working than the 9-CRFS.

With these systems, it is now possible to grow several cultures in parallel under the same external conditions (temperature, media, time, pressure gradient), making the initial state of gels or cells reproducible. This is very useful for lymphatic and blood angiogenesis resarch as the effects of different growth factors or inhibitors on cell morphogenesis and structure formation can be compared, as well as synergistic effects between flow and signaling molecules, which we showed here (Fig. 13). However, these tools are not only limited to angiogenesis assays. Any effect of the combination of two or more of the following elements can be observed: different cell types, flow, matrix composition or morphogens. The three experiments carried out in this project (effect of flow and VEGF on angiogenesis, lymph node metastasis and fibroblast-tumor cell co-culture and their effect on the matrix) show the versatility of the chambers. Other examples would be gel extraction for analysis of the factors secreted by the cells, in the absence or presence of flow, or testing the effect of incorporated factors in the gel or different concentrations of collagen or fibrin on cells. The media is in direct contact with the gel, reducing barriers for penetration studies, such as those done with nanoparticles, which is not possible in the single-chamber system for example, because of the hydrophilic porous polyethylene at the inlet. Finally, not only do these powerful and versatile interstitial flow devices bring *in vitro* studies one step closer

to the complexity of *in vivo* experiments by including a third dimension and flow, they allow fine tuning of the applied conditions. This is an important feature in understanding key players and testing hypothesis for potential future therapeutical applications in lymphangiogenesis or cancer for example.

6 Conclusion

The role of interstitial flow on cell dynamics is significant: it can help cells grow and organize, influence migration and deliver molecules to or create gradients around cells. Understanding by which means interstitial flow leads to these events and how changes in the extracellular matrix and its components affect cells is key to finding therapeutics for many pathologies, such as lymphedema, infection, inflammation or cancer. The first step towards providing these answers lies in mimicking the *in vivo* environment of cells, i.e. through 3D fluidic devices. We have developed two efficient tools to study the significant influence of the microenvironment on cells. The successful *in vitro* angiogenesis assay together with the proof of principle experiments for other cell behaviors show the usefulness and versatility of these systems. Their advantageous feature is their multiple identical chambers. With minimal setup, we are capable of recreating nine or ten identical environments in order to test the effect of variations in the microenvironment. With these systems, we will be able to study a wide range cell-microenvironment interactions with a higher throughput than existing devices, and with potential therapeutical applications.

7 Acknowledgments

I would like thank Prof. Melody Swartz for giving me the possibility to accomplish this master project in her lab. It was an exciting and enriching opportunity. A special thanks to Adrian Shieh for guiding me during my project. Finally, I would like to thank all the LLCB members, in particular Didier Foretay, Ulrike Haessler and Brandon Dixon, and Jan Overney from LCSB1, for their help.

References

[1] D. Axelrod, D. E. Koppel, J. Schlessinger, E. Elson, and W. W. Webb. Mobility measurement by analysis of fluorescence photobleaching recovery kinetics. *Biophys J*, 16(9):1055–69, 1976.

[2] D. A. Berk, M. A. Swartz, A. J. Leu, and R. K. Jain. Transport in lymphatic capillaries. ii. microscopic velocity measurement with fluorescence photobleaching. *Am J Physiol*, 270(1 Pt 2):H330–7, 1996.

[3] K. S. Blum, C. Hadamitzky, K. F. Gratz, and R. Pabst. Effects of autotransplanted lymph node fragments on the lymphatic system in the pig model. *Breast Cancer Res Treat*, 2009.

[4] K. C. Boardman and M. A. Swartz. Interstitial flow as a guide for lymphangiogenesis. *Circ Res*, 92(7):801–8, 2003.

[5] C. Bonvin, J. Overney, A. C. Shieh, J. B. Dixon, and M. A Swartz. A multichamber fluidic device for 3d cultures with examples in capillary morphogenesis and fibroblast-tumor cell co-culture. *Biotechnol Bioeng*, to be submitted.

[6] R. Cailleau, M. Olive, and Q. V. Cruciger. Long-term human breast carcinoma cell lines of metastatic origin: preliminary characterization. *In Vitro*, 14(11):911–5, 1978.

[7] S. R. Chary and R. K. Jain. Direct measurement of interstitial convection and diffusion of albumin in normal and neoplastic tissues by fluorescence photobleaching. *Proc Natl Acad Sci U S A*, 86(14):5385–9, 1989.

[8] S. Chung, R. Sudo, P. J. Mack, C. R. Wan, V. Vickerman, and R. D. Kamm. Cell migration into scaffolds under co-culture conditions in a microfluidic platform. *Lab Chip*, 9(2):269–75, 2009.

[9] H. Dafni, T. Israely, Z. M. Bhujwalla, L. E. Benjamin, and M. Neeman. Overexpression of vascular endothelial growth factor 165 drives peritumor interstitial convection and induces lymphatic drain: magnetic resonance imaging, confocal microscopy, and histological tracking of triple-labeled albumin. *Cancer Res.*, 62(22):6731–9, 2002.

[10] M. E. Fleury, K. C. Boardman, and M. A. Swartz. Autologous morphogen gradients by subtle interstitial flow and matrix interactions. *Biophys J*, 91(1):113–21, 2006.

[11] L. G. Griffith and M. A. Swartz. Capturing complex 3d tissue physiology in vitro. *Nat Rev Mol Cell Biol*, 7(3):211–24, 2006.

[12] B. M. Gumbiner. Cell adhesion: the molecular basis of tissue architecture and morphogenesis. *Cell*, 84(3):345–57, 1996.

[13] U. Haessler, Y. Kalinin, M. A. Swartz, and M. Wu. An agarose-based microfluidic platform with a gradient buffer for 3d chemotaxis studies. *Biomed Microdevices*, 2009.

[14] C. L. Helm, M. E. Fleury, A. H. Zisch, F. Boschetti, and M. A. Swartz. Synergy between interstitial flow and vegf directs capillary morphogenesis in vitro through a gradient amplification mechanism. *Proc Natl Acad Sci U S A*, 102(44):15779–84, 2005.

[15] C. L. Helm, A. Zisch, and M. A. Swartz. Engineered blood and lymphatic capillaries in 3-d vegf-fibrin-collagen matrices with interstitial flow. *Biotechnol Bioeng*, 96(1):167–76, 2007.

[16] R. Hernandez Vera, E. Genove, L. Alvarez, S. Borros, R. Kamm, D. Lauffenburger, and C. E. Semino. Interstitial fluid flow intensity modulates endothelial sprouting in restricted src-activated cell clusters during capillary morphogenesis. *Tissue Eng Part A*, 15(1):175–85, 2009.

[17] R. K. Jain. Transport of molecules, particles, and cells in solid tumors. *Annu. Rev. Biomed. Eng.*, 1:241–63, 1999.

[18] M. S. Kolodney and R. B. Wysolmerski. Isometric contraction by fibroblasts and endothelial cells in tissue culture: a quantitative study. *J Cell Biol*, 117(1):73–82, 1992.

[19] S. P. Leong, B. Cady, and D. M. et al. Jablons. Clinical patterns of metastasis. *Cancer Metastasis Rev.*, 25(2):221–32, 2006.

[20] N. Loren, M. Nyden, and A. M. Hermansson. Determination of local diffusion properties in heterogeneous biomaterials. *Adv Colloid Interface Sci*, 2009.

[21] A. Muller, B. Homey, H. Soto, N. Ge, D. Catron, M. E. Buchanan, T. McClanahan, E. Murphy, W. Yuan, S. N. Wagner, J. L. Barrera, A. Mohar, E. Verastegui, and A. Zlotnik. Involvement of chemokine receptors in breast cancer metastasis. *Nature*, 410(6824):50–6, 2001.

[22] C. P. Ng, C. L. Helm, and M. A. Swartz. Interstitial flow differentially stimulates blood and lymphatic endothelial cell morphogenesis in vitro. *Microvasc Res*, 68(3):258–64, 2004.

[23] C. P. Ng, B. Hinz, and M. A. Swartz. Interstitial fluid flow induces myofibroblast differentiation and collagen alignment in vitro. *J Cell Sci*, 118(Pt 20):4731–9, 2005.

[24] C. P. Ng and S. H. Pun. A perfusable 3d cell-matrix tissue culture chamber for in situ evaluation of nanoparticle vehicle penetration and transport. *Biotechnol Bioeng*, 99(6):1490–501, 2008.

[25] C. P. Ng and M. A. Swartz. Fibroblast alignment under interstitial fluid flow using a novel 3-d tissue culture model. *Am J Physiol Heart Circ Physiol*, 284(5):H1771–7, 2003.

[26] W. L. Olszewski. The lymphatic system in body homeostasis: physiological conditions. *Lymphat Res Biol*, 1(1):11–21; discussion 21–4, 2003.

[27] J. A. Pedersen and M. A. Swartz. Mechanobiology in the third dimension. *Ann Biomed Eng*, 33(11):1469–90, 2005.

[28] R. Peters, J. Peters, K. H. Tews, and W. Bahr. A microfluorimetric study of translational diffusion in erythrocyte membranes. *Biochim Biophys Acta*, 367(3):282–94, 1974.

[29] S. Podgrabinska, P. Braun, P. Velasco, B. Kloos, M. S. Pepper, and M. Skobe. Molecular characterization of lymphatic endothelial cells. *Proc Natl Acad Sci U S A*, 99(25):16069–74, 2002.

[30] S. Rhee, H. Jiang, C. H. Ho, and F. Grinnell. Microtubule function in fibroblast spreading is modulated according to the tension state of cell-matrix interactions. *Proc Natl Acad Sci U S A*, 104(13):5425–30, 2007.

[31] J. M. Rutkowski, M. Moya, J. Johannes, J. Goldman, and M. A. Swartz. Secondary lymphedema in the mouse tail: Lymphatic hyperplasia, vegf-c upregulation, and the protective role of mmp-9. *Microvasc Res*, 72(3):161–71, 2006.

[32] J. M. Rutkowski and M. A. Swartz. A driving force for change: interstitial flow as morphoregulator. *Trends Cell Biol.*, 17(1):44–50, 2007.

[33] C. E. Semino, R. D. Kamm, and D. A. Lauffenburger. Autocrine egf receptor activation mediates endothelial cell migration and vascular morphogenesis induced by vegf under interstitial flow. *Exp Cell Res*, 312(3):289–98, 2006.

[34] J. D. Shields, M. E. Fleury, C. Yong, A. A. Tomei, G. J. Randolph, and M. A. Swartz. Autologous chemotaxis as a mechanism of tumor cell homing to lymphatics via interstitial flow and autocrine ccr7 signaling. *Cancer Cell*, 11(6):526–38, 2007.

[35] C. L. Stokes and D. A. Lauffenburger. Analysis of the roles of microvessel endothelial cell random motility and chemotaxis in angiogenesis. *J Theor Biol*, 152(3):377–403, 1991.

[36] R. Sudo, S. Chung, I. K. Zervantonakis, V. Vickerman, Y. Toshimitsu, L. G. Griffith, and R. D. Kamm. Transport-mediated angiogenesis in 3d epithelial coculture. *Faseb J*, 2009.

[37] M. A. Swartz. The physiology of the lymphatic system. *Adv Drug Deliv Rev*, 50(1-2):3–20, 2001.

[38] M. A. Swartz, J. A. Hubbell, and S. T. Reddy. Lymphatic drainage function and its immunological implications: from dendritic cell homing to vaccine design. *Semin Immunol*, 20(2):147–56, 2008.

[39] N. J. Tawil, V. Gowri, M. Djoneidi, J. Nip, S. Carbonetto, and P. Brodt. Integrin alpha3beta1 can promote adhesion and spreading of metastatic breast carcinoma cells on the lymph node stroma. *Int J Cancer*, 66(5):703–10, 1996.

[40] A. A. Tomei, S. Siegert, M. R. Britschgi, S. A. Luther, and M. A. Swartz. Fluid flow regulates stromal cell organization and ccl21 expression in a tissue-engineered lymph node microenvironment. *Journal of Immunology*, in revision.

[41] V. Vickerman, J. Blundo, S. Chung, and R. Kamm. Design, fabrication and implementation of a novel multi-parameter control microfluidic platform for three-dimensional cell culture and real-time imaging. *Lab Chip*, 8(9):1468–77, 2008.

[42] S. Wang and J. M. Tarbell. Effect of fluid flow on smooth muscle cells in a 3-dimensional collagen gel model. *Arterioscler Thromb Vasc Biol*, 20(10):2220–5, 2000.

[43] K. M. Yamada and E. Cukierman. Modeling tissue morphogenesis and cancer in 3d. *Cell*, 130(4):601–10, 2007.

[44] M. Yilmaz, G. Christofori, and F. Lehembre. Distinct mechanisms of tumor invasion and metastasis. *Trends Mol Med.*, 13(12):535–41, 2007.

[45] A. H. Zisch, U. Schenk, J. C. Schense, S. E. Sakiyama-Elbert, and J. A. Hubbell. Covalently conjugated vegf–fibrin matrices for endothelialization. *J Control Release*, 72(1-3):101–13, 2001.

8 Appendix

8.1 Appendix 1: 9-chamber radial flow chamber protocol

Molding the system

- Clean mold well with kim-wipes, removing all remaining PDMS from previous injections
- Soak mold in soap water (1tsp in 300 ml of water) for 25 minutes
- Prepare 7 ml of PDMS per mold (1:10 by weight), mix well and degas in vacuum oven until no more bubbles
- Remove mold from soapy water and blow-dry with compressed air
- Assemble mold, screwing by hand (do not screw to tight to avoid breaking the mold)
- Cut off tip a 1 ml pipette tip with a razor blade
- Fill a 10 ml syringe with 7 ml of degassed PDMS avoiding air bubbles
- Drip PDMS into filling port, put the pipette tip on syringe and prime
- Insert syringe/pipette tip into port and fill mold slowly holding mold with air exits upwards
- Wipe off excess PDMS from the mold, and pour an extra drop of PDMS onto filling port. This will help to remove the system
- Once filled, bake in oven for 1h30min at 90°C, or overnight at 60°C
- Remove system while the PDMS and mold are still warm (but not too hot, or the PDMS will tear easily). To remove the system, use razor blade to separate both parts of the mold. Pull and break PDMS bubble that has formed on top of filling port. This liberates the filling port. Use compressed air nozzle at maximum power and blow into filling port. The system will start to detach. If the PDMS that was in the air exits is still linked to the system, cut it with a razor blade. Do not rip off, as this will create a dent and weaken the system at that spot. If a minor tear happens in an area which is not important for the flow profile (in an unused chamber or along the sides), add a little bit of unpolymerized PDMS and rebake in oven
- Drill necessary holes in the system
- Use scotch tape to remove any excess material from the system
- Autoclave flow system and PE rings

Assembling the system

- Prepare glass by washing with soap. Wash with alcohol, then acetone: dip kim-wipe in alcohol or acetone respectively and wipe both sides of glass. Dry (air or kim-wipe)
- Under the hood, insert PE rings in chambers and close with glass coverslip. PE rings sometimes insert better in one direction than the other. Press PDMS and glass together until they bind. Can use a small Petri dish to press on the whole system, and then use forceps to press between each chamber and in the center. Make sure you can still detach the glass from the Petri dish before leaving the hood
- Plasma treat glass and PDMS stuck together (with PE rings) or separate at 200W for 1 minute
- Once out of oven, press PDMS and glass together until they bind (same as when assembling the system)

Surface treatment

- Fill chambers with poly-L-lysine (if possible only within PE ring) making sure that the setup is completely tight. The liquid must fill the compartment entirely so the top surface is treated as well (volume = 40 μl). Let sit for minimum 25 minutes at RT.
- Remove poly-L-lysine and rinse with mQ-H_2O once and add glutaraldehyde (0.1%). Let sit for maximum 25 minutes at RT
- Rinse 6 times with mQ-H_2O
- Can store system for 1-3 days. Fill all chambers with mQ-H_2O and place wet kim-wipe on top of system. Parafilm Petri dish and store at 4°C

Filling the chamber

- Remove all water from chambers, dry in vacuum oven for 1h
- Fill chambers immediately. When filling, use either yellow tips (200μl) or filling tips. Gel should be only within the PE ring, but must also make sure the gel has filled to the top of the chamber. If a little bit of gel leaks out of PE ring, it is ok, as long as it does not fill the surrounding chamber.
- Let gel polymerize for 20 minutes at 37°C. Add media, first in static conditions (fill both rings to the top) for 12-24h, then inflow (fill outer ring more than inner ring, but must make sure there is some media in the outlets as well)
- Sometimes, air gets trapped between outer edge of PE ring and PDMS. To remove air bubbles, use high gage needle (26G) and a 5 ml syringe. Poke needle into bubble

through PDMS and aspirate air. The PDMS will close again once the needle is withdrawn

8.2 Appendix 2: multi-chamber migration assay protocol

Molding the system

- Clean mold well with kim-wipes, removing all remaining PDMS from previous injection
- Soak mold in soap water (1tsp in 300 ml of water) for 25 minutes
- Prepare 7 ml of PDMS per mold (1:10 by weight), mix well and degas in vacuum oven until no more bubbles
- Remove mold from soapy water and blow-dry with compressed air
- Pour some PDMS on the part of the mold that has the chambers and put in vacuum for 30 minutes. This will allow PDMS to enter the little holes, otherwise no pillars will be present
- Assemble mold, screwing by hand (do not screw to tight to avoid breaking the mold)
- Cut off tip of a 1 ml pipette tip with a razor blade
- Fill a 10 ml syringe with PDMS avoiding air bubbles
- Drip PDMS into filling port, put the pipette tip on syringe and prime
- Insert syringe/pipette tip into port and fill mold slowly holding mold with air exits upwards
- Wipe off excess PDMS from the mold, and pour an extra drop of PDMS onto filling port. This will help to remove the system
- Once filled, bake in oven for 1h30min at 90°C
- Remove system while the PDMS and mold are still warm (but not too hot, or the PDMS will tear easily). To remove the system, use razor blade to separate both parts of the mold. Pull and break PDMS bubble which has formed on top of filling port. Lift outer edge of the PDMS and pull until the PDMS come out of the mold (always separate edge near air exits last, to prevent tears) If the PDMS that was in the air exits is still linked to the reservoirs, cut it with a razor blade. Do not rip off, as this will create a dent and weaken the system at that spot.
- Drill necessary holes in PDMS (2 filling holes in each side chamber, 2 in the central chamber and one big hole as the inlet)
- With a razor blade, cut outer outlets or drill top outlets
- Use scotch tape to remove any excess material from the system

- Autoclave flow system

Assembling the system

- Prepare glass by washing with soap. Wash with alcohol, then acetone: dip kim-wipe in alcohol or acetone respectively and wipe both sides of glass. Dry (air or kim-wipe)
- Under the hood, close PDMS unit with glass coverslip. Press PDMS and glass together until they bind. Can use a small Petri dish to press on the whole system, and then use forceps to press between each individual chamber and on the sides. Make sure you can still detach the glass from the Petri dish before leaving the hood
- Plasma treat glass and PDMS stuck together (with PE rings) or separate at 200W for 1 minute
- Once out of oven, press PDMS and glass together until they bind (same as when assembling the system)

Surface treatment

- Fill chambers (use filling tips) with poly-L-lysine (if possible only within PE ring) making sure that the setup is completely tight. The liquid must fill all compartments that will contain gel entirely so the top surface is treated as well (volume = 20 μl for the side chambers, 160 μl for the central chamber). Let sit for minimum 25 minutes at RT.
- Remove poly-L-lysine and rinse with mQ-H_2O once and add glutaraldehyde (0.1%). Let sit for maximum 25 minutes at RT
- Rinse 6 times with mQ-H_2O
- Can store system for 1-3 days. Fill all chambers with mQ-H_2O and place wet kim-wipe on top of chamber. Parafilm Petri dish and store at 4°C.

Surface treatment

- Remove all water from chambers and dry in vacuum oven for 1h
- Fill chambers immediately. When filling, use filling tips. First fill the central chamber then immediately fill side chambers. Let gel polymerize for 20 minutes at 37°C.
- If needed, close filling ports with agarose. Let set at 37°C for 20 minutes.
- Add media, first in static conditions (fill both inside and outside of ring) for 12-24h, then in flow (remove media from around the chamber)
- To remove air bubbles from the outlets, use high gage needle (26G) and a 5 ml syringe. Poke needle into bubble through PDMS and aspirate air. The PDMS will close again once the needle is withdrawn

8.2: Appendix 3: Matlab script for FRAP analysis, written by Brandon Dixon

```
clear;

cd '/Users/carmen/Desktop/FRAP angio 061509.mdb/chamber312p2'

pixelsize=.9; % in um/pixel
deltat=3.93; % in sec
prebleach=double(imread('chamber312p2_t01.TIF')); %any image before
bleaching
startat=input('Enter in the image number of the first bleached image:
');
endon=input('Enter the image number you want to end on: ');
pic=imread('chamber312p2_t02.TIF'); %first bleached image
% Pic=pic(:,:,2);
figure;
imagesc(pic);
[xi,yi,P]=impixel;
pic=imcrop(pic,[xi-64 yi-64 127 127]);
level=graythresh(pic);
bwpic=im2bw(pic,level);
bwpic=not(bwpic);
se1=strel('disk',5);
bwpic=imerode(bwpic,se1);
bwpic=imfill(bwpic,'holes');
bwpic=bwlabel(bwpic);
temp=regionprops(bwpic,'Centroid');
xi=xi+round(temp(bwpic(64,64)).Centroid(1)-64.5);
yi=yi+round(temp(bwpic(64,64)).Centroid(2)-64.5);


for x=startat:endon
    if x < 10
      addzero='0'; %add a 0 if series is bigger than 100
      str2=strcat(addzero,num2str(x));
%     elseif x >= 10 & x < 100
%       addzero='0';
%       str2=strcat (addzero,num2str(x));
    else
      str2=num2str(x);
    end
    pic=imread(strcat('chamber312p2_t', str2, '.tif'));
    pic=double(pic)-prebleach;
    pic=imcrop(pic,[xi-256 yi-256 511 511]);
    imagesc(pic);
    F(x-startat+1)=getframe;
    fftpic=fft2(double(pic));
    Iqx(x-startat+1)=fftpic(1,2);
    Iqy(x-startat+1)=fftpic(2,1);
end
```

```
temp=acos(real(Iqx)./abs(Iqx))/2/pi*512*pixelsize;
temp1=temp';
t=0:deltat:deltat*(endon-startat);
t=t';
XX=[ones(size(t)) t];
xvel=XX\temp1;
xvel=-xvel(2)
temp=acos(real(Iqy)./abs(Iqy))/2/pi*512*pixelsize;
temp2=temp';
yvel=XX\temp2;
yvel=-yvel(2)
totvel=sqrt(xvel.^2+yvel.^2)
figure; plot(temp1, temp2, '*'); xlabel('x displacement'); ylabel('y
displacement'); title('x vs y');
figure; plot(temp1, '*'); xlabel('image number'); ylabel('x
displacement'); title ('x=f(t)');
figure; plot(temp2, '*'); xlabel('image number'); ylabel('y
displacement'); title ('y=f(t)');
```